Apparatus and method to recover the Mueller matrix in bright-field microscopy

Sofia Obando-Vasquez, Ana Doblas and Carlos Trujillo

Citation: American Journal of Physics **90**, 702 (2022); doi: 10.1119/5.0081673
View online: https://doi.org/10.1119/5.0081673
View Table of Contents: https://aapt.scitation.org/toc/ajp/90/9
Published by the American Association of Physics Teachers

INSTRUCTIONAL LABORATORIES AND DEMONSTRATIONS

John Essick, *Editor*

Department of Physics, Reed College, Portland, OR 97202

Articles in this section deal with new ideas and techniques for instructional laboratory experiments, for demonstrations, and for equipment that can be used in either. Although these facets of instruction also appear in regular articles, this section is for papers that primarily focus on equipment, materials, and how they are used in instruction. Manuscripts should be submitted using the web-based system that can be accessed via the American Journal of Physics home page, ajp.aapt.org, and will be forwarded to the IL&D editor for consideration.

Apparatus and method to recover the Mueller matrix in bright-field microscopy

Sofia Obando-Vasquez
Applied Optics Group, School of Applied Science and_ Engineering, Universidad EAFIT, MedellÃn, Colombia

Ana Doblas[a)]
Department of Electrical and Computer Engineering, The University of Memphis, Memphis, Tennessee 38152

Carlos Trujillo[b)]
Applied Optics Group, Physical Sciences Department, Universidad EAFIT, MedellÃn, Colombia

(Received 9 December 2021; accepted 10 June 2022)

We present a simple experiment developed for the advanced physics instructional laboratory to calculate the Mueller matrix of a microscopic sample. The Mueller matrix is obtained from intensity-based images of the sample acquired by a polarization-sensitive microscope. The experiment requires a bright-field microscope and standard polarizing optical components such as linear polarizers and waveplates. We provide a practical procedure for implementing the apparatus, measuring the complete Mueller matrix of linear polarizers used as samples, and discuss the possibility of analyzing biological samples using our apparatus and method. Due to the simplicity of the apparatus and method, this experiment allows students to increase their knowledge about light polarization and initiate their training in optical instrumentation.

https://doi.org/10.1119/5.0081673

I. INTRODUCTION

Visible light is an electromagnetic wave in which electric and magnetic fields oscillate perpendicularly to the direction of propagation. When the electric field oscillation is well defined over time, light is said to be polarized. Depending on how the electric field is oriented, the polarization state of light can be classified as linear, circular, or elliptical polarization. The latter type of polarization provides the most general description of polarized light. Polarization is a standard topic in undergraduate physics courses, which are focused on the wave properties of light.[1]

Polarization can be useful in a variety of imaging applications. In photography, the insertion of polarizers in imaging systems reduces glare from light scattering, increases contrast, eliminates hot spots from reflective objects, and detects hidden image features.[2] Polarization is also used to evaluate stress in amorphous solids such as glass and plastic.[3] Stress from temperature and pressure profiles in birefringent and nonhomogeneous materials introduces localized variations and gradients of the material properties. This stress can be observed and quantified in transparent objects using polarized light methodologies[4] due to the localized changes in the refractive index.[5] Polarization has also been used in the chemical, pharmaceutical, and food and beverage industries, enabling the detection and quantification of the chemical compounds. Many organic chemical compounds (including active pharmaceutical ingredients and sugars) are optically active, rotating the polarization state of the light in different directions based on their nature and concentration.[1] Polarimetry has also provided a vast number of applications in different fields of astrophysics from solar physics to cosmology. For example, polarimetry allows the description and measurement of magnetic fields of astrophysical objects (intensity and orientation), quantities that cannot be measured directly.[6]

Polarization has also been used in microscopy.[7–9] In a simple polarization microscope system, two linear polarizers are inserted. The first polarizer is inserted in front of the illumination source to polarize the incident light linearly, whereas the second polarizer is set in front of the sensor (commonly known as the analyzer).[10] The transmission axis of the analyzer is rotated at 90° to the transmission axis of the first polarizer. If an anisotropic or birefringent specimen is inserted between the crossed polarizers, the specimen produces two perpendicular wave components (ordinary and extraordinary wavefronts) with a phase difference between them. These wavefronts are then recombined by constructive and destructive interference at the analyzer.[1] In such a configuration, the analyzer only transmits light that has experienced a specimen-induced phase shift between the perpendicular components and continues to block all the light from the source initially polarized by the first polarizer. The resulting high-contrast intensity is proportional to the specimen thickness and birefringence.[11] Since many biological samples, including cancer cells[12,13] and tendons,[14] are intrinsically birefringent, polarization-sensitive microscopy has been a hot topic in biological studies over the last decades. Polarization-sensitive microscopy has enabled the detection and screening of diseases by analyzing the polarimetric properties of biological samples. In 2009, Palacios *et al.* compared the capability of different techniques for extracting information from biological samples,[15] concluding that polarization-sensitive techniques provide more information than nonpolarization approaches to the study of biological and inorganic samples. In 2015, Pirnstill and Cot developed a cheap, portable polarization microscope for detecting malaria in blood samples using a cell phone.[16] In 2018, Wang *et al.* studied the change in the birefringence in bladder normal and cancerous tissue.[12]

Due to the wide-ranging application of light polarization in many important fields, educators introduce students to the fundamentals of this topic in basic instructional and research activities. Several polarization experiments are commonly taught in the introductory optical laboratory: verification of Malus' law,[17] measurement of the Brewster angle for the glass–air interface,[18] computation of the Stokes parameters,[19] and retrieval of the reflected and transmitted waves' polarization characteristics.

Polarization-based techniques are commonly based on estimating the Jones or Mueller matrices of the studied samples. While the estimation of the Jones matrix requires an optical interferometer,[20] the Mueller matrix can be calculated directly from intensity-based images,[21] resulting in a more straightforward optical configuration. Another advantage of the Mueller formalism is its applicability to polarized and depolarized light.[22] Using the Mueller formalism, the sample's birefringence, diattenuation, and depolarization can be estimated. These parameters represent a biological sample's polarization properties.[23]

In this paper, we present a complete method for estimating the Mueller matrix from intensity-based measurements. We also provide a detailed description of the required experimental system, including alignment procedures and software tools, so that students can carry out a measurement of a sample's polarimetric properties. First, we present the alignment protocol to convert a brightfield microscope into a polarization-sensitive microscope by inserting a polarization state generator (PSG) and a polarization state analyzer (PSA). Then, we use our system to study the polarizing properties of a linear polarizer whose transmission axis is oriented at 0°, +45°, and 90° with respect to the PSG and two biological samples. The proposed method for obtaining the Mueller matrix only requires conventional optical elements in a simple arrangement, making it easy to implement and use. The system is a valuable educational tool, providing students useful experience with the polarization properties of light.

II. DESCRIPTION OF APPARATUS AND METHOD

This section describes the apparatus and method we use to estimate the Mueller matrix for a sample, where the sample's polarization properties vary across its transverse field of view.

A. Apparatus to record the intensity-based images

In this particular case, the estimation of the Mueller matrix is based on the recording of 36 intensity-based images using a brightfield microscope. Figure 1 shows the optical configuration of the brightfield microscope using a collimated beam. A sample is imaged using an infinity-corrected microscope objective (MO) lens, which forms the image of the sample at the infinity. Thus, to produce a real sample image, one must

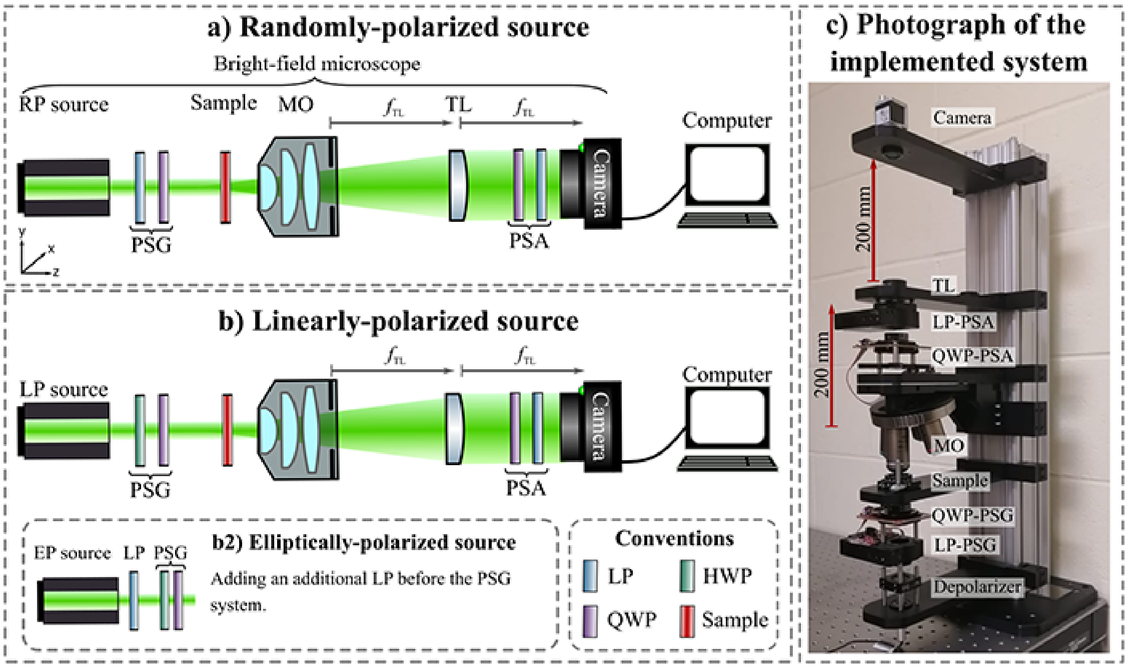

Fig. 1. (a) and (b) Illustration of the optical configurations for the apparatus according to the illumination source polarization state. (c) A labeled photograph of the implemented system with the relevant distances between optical elements. The laser source is located at the bottom of the system in the photograph.

insert a tube lens (TL). Under this configuration, the microscope's image plane is located at the back focal plane (bfp) of the TL lens. The digital sensor (i.e., a CCD or CMOS camera) is placed at the bfp of the TL to ensure that focused images are recorded. The distance between the MO and TL is such that the telecentric regime is guaranteed (e.g., afocal configuration).

To convert the brightfield microscope into a polarization-sensitive microscope, we insert polarization state generator (PSG) and polarization state analyzer (PSA) systems before the sample and after the TL, respectively. While the PSA system is always composed of a quarter-wave plate (QWP) followed by a linear polarizer (LP), the PSG system depends on the polarization state of the illumination source. To check the polarization state of the source, insert and rotate a LP right after the illumination source. If the intensity of the emerging light remains invariant to the rotation of the LP, the source is randomly polarized. Otherwise, the source is elliptically polarized.

When using a randomly polarized source [Fig. 1(a)], the PSG system comprises a LP followed by a QWP. For linearly polarized sources, the PSG system is composed of a half-wave plate (HWP) followed by a QWP [Fig. 1(b)]. Finally, for elliptically polarized sources, an LP can be inserted before the HWP and the QWP [the inset in Fig. 1(b)]. The transmission axis of the LP must be aligned with the major axis of the polarization state of the source to ensure the highest intensity of the beam. The alignment of this additional LP is performed by rotating the LP until the maximum intensity of the emerging beam is observed. Alternatively, one can use a depolarizer instead of the additional LP, converting the elliptically polarized source into a randomly polarized source. Therefore, the PSG is the same as the randomly polarized case [Fig. 1(a)].

The next step is the alignment of the PSG and PSA systems. The alignment procedure depends on the polarizing elements used for the PSG and the PSA systems. First, we describe the alignment protocol of the polarizing elements when using a randomly polarized source. Before aligning the elements, a calibrated LP is needed. If there is no such element in the laboratory, a LP can be calibrated using a linearly polarized source.

The general procedure for calibrating a LP is to place it after the beam emerges from the source and rotate the LP until its minimum intensity is found. This minimum can be checked effortlessly by observing a histogram of the recorded image. (Usually, commercial camera software provides the histogram of the current acquisition.) There are two orientations in which the intensity is minimum: at 90° or 270° with respect to the orientation of the source. In either of these two orientations for the LP, its transmission axis is orthogonal to the polarization axis of the source. For example, if the source is vertically polarized (say, perpendicular to the laboratory table plane), the LP transmission axis is horizontal (say, parallel to the laboratory table plane). After calibrating the LP, this polarizer is inserted after the randomly polarized source and set in a fixed orientation. The orientation of the calibrated LP must not be a specific one; it could be either vertical, horizontal, or otherwise. Nevertheless, this orientation must be kept invariant during the alignment protocol since it refers to the zero reference of the whole system.

Next, insert the LP of the PSA system (LP-PSA). The orientation of the LP-PSA is such that the intensity of the beam recorded by the camera is minimum. This orientation remains fixed throughout the alignment protocol. The next element to align is the LP of the PSG system (LP-PSG). Before inserting the LP-PSG, the calibrated polarizer is removed from the microscope path; thus, only the LPs of the PSG and PSA systems are kept in the setup. The orientation of the LP-PSG is such that the intensity of the beam recorded by the camera is minimum. This orientation is fixed during the rest of the alignment procedure. Now, insert the QWP-PSG after the LP-PSG and before the sample. Rotate the QWP-PSG until the recorded intensity is minimum. There are two orientations of the fast axis of the QWP-PSG that generate a minimum intensity: 0° and 90° with respect to the transmission axis of LP-PSG. Choose the one in which the QWP's fast axis is parallel to the transmission axis of the LP-PSG. Now, insert the QWP-PSA before the LP-PSA. The orientation of the QWP-PSA is such as to guarantee: (1) it generates a minimum intensity at the camera and (2) its fast axis is parallel to the transmission axis of the LP-PSG. Finally, rotate the LP-PSA 90° clockwise.

The alignment protocol is slightly different if the source is linearly polarized. If the direction of the polarization state of the source is known, there is no need to use a calibrated LP. The first element to be aligned is the LP-PSA. Assuming that the orientation of the polarization state of the source is known, the orientation of the LP-PSA is such that the intensity of the beam recorded by the camera is minimum. The next element to be set and aligned is the HWP-PSG. Its orientation is such that the intensity of the recorded beam is minimum. Although two HWP-PSG orientations are generating a minimum intensity (i.e., 0° and 180° to the orientation of the source), both are always parallel to the polarization state of the source. Next, insert the QWP-PSG after the HWP-PSG. The orientation of the QWP-PSG is such that: (1) the intensity of the beam recorded by the camera is minimum and (2) the orientation of the QWP-PSG's fast axis is parallel to the transmission axis of the source. Finally, insert the QWP-PSA before the LP-PSA. The QWP-PSA is oriented with the same restrictions as the QWP-PSG. Once all the polarizing elements are aligned, rotate the LP-PSA 90° clockwise.

Suppose the source is elliptically polarized [the inset of Fig. 1(b)]. In that case, an additional LP is inserted after the source, and the same alignment protocol as when the source was linearly polarized is followed. Alternatively, a depolarizer can be used instead of the LP. In this case, the alignment of the system is the same as the one for a randomly polarized source. If using the LP, consider the most general case in which the elliptical polarization state is unknown. There are three different approaches to aligning this additional LP. In the first case, the orientation of the transmission axis of the LP is at 0° or 90°. Insert the LP after the source and rotate the source to obtain the maximum intensity after the calibrated LP (e.g., alignment of the ellipse's major axis to the transmission axis of the LP). If the source cannot be rotated, the second possibility is to rotate the calibrated LP to align its transmission axis parallel to the major axis of the ellipse of the source. As the transmission axis of the calibration LP has been rotated, the polarizing elements of the microscope must be aligned accordingly. The last and simplest option involves inserting a calibrated LP with its transmission axis oriented either at 0° or 90° without rotating the source. This option is only recommended if the source's intensity is strong enough, so losing intensity is not a concern throughout the microscope.

Once the system is aligned (regardless the type of the source's polarization state), we record 36 required intensity-based images by rotating the polarizing elements of both PSG and PSA systems. Using these 36 intensity-based images, we estimate the sample's Muller matrix. In our method, the following polarization states in both PSG and PSA systems must be generated: vertical polarization, i.e., 90° (V), horizontal polarization, i.e., 0° (H), linear polarization at +45° (P), linear polarization at −45° (M), right-handed circular polarization (R), and left-handed circular polarization (L). The orientation angles of the polarizing elements of the PSG and PSA systems to their reference zero (i.e., the orientation angles obtained during the alignment procedure) are found in Appendix B. To ease the applicability of the proposed apparatus and method, we have provided the orientation angles when the source is randomly polarized and elliptically polarized. The insertion of all the latter polarizing elements in the proposed apparatus does not produce any vignetting effects in the recorded images since these elements do not act as the microscope's entrance and exit pupils.

B. Method to estimate the Mueller matrix

Several methods have been reported to calculate the 16 elements of the Mueller matrix for a random sample based on recording multiple intensity-based images ranging from 16 up to 49 images.[24,25] The fewer the number of images, the less acquisition time is required. Nonetheless, those methods are prone to inaccuracies. On the contrary, the methods requiring more images provide higher accuracy and less noise sensitivity since each element of the Mueller matrix is overestimated.[26] There must be a tradeoff between the number of images and the acquisition time. Therefore, we propose the method that requires 36 images[25] since it balances this tradeoff providing accurate results with a reduced number of images (36 versus 49 images). The 36 intensity-based images are recorded by changing the polarization state of both the polarization state generator (PSG) and polarization state analyzer (PSA) systems (see Sec. II A and Appendix B). Based on these polarization states of PSG and PSA systems, the Mueller matrix, M, is

$$M = \begin{bmatrix} m_{00} & m_{01} & m_{02} & m_{03} \\ m_{10} & m_{11} & m_{12} & m_{13} \\ m_{20} & m_{21} & m_{22} & m_{23} \\ m_{30} & m_{31} & m_{32} & m_{33} \end{bmatrix}. \tag{1}$$

In Eq. (1),[25] each element of the Mueller matrix is estimated by pointwise adding or subtracting four of the 36 images

$$\begin{aligned} m_{00} &= HH + HV + VH + VV, & m_{01} &= HH + HV - VH - VV, \\ m_{02} &= PH + PV - MH - MV, & m_{03} &= RH + RV - LH - LV, \\ m_{10} &= HH - HV + VH - VV, & m_{11} &= HH - HV - VH + VV, \\ m_{12} &= PH - PV - MH + MV, & m_{13} &= RH - RV - LH + LV, \\ m_{20} &= HP - HM + VP - VM, & m_{21} &= HP - HM - VP + VM, \\ m_{22} &= PP - PM - MP + MM, & m_{23} &= RP - RM - LP + LM, \\ m_{30} &= HR - HL + VR - VL, & m_{31} &= HR - HL - VR + VL, \\ m_{32} &= PR - PL - MR + ML, & m_{33} &= LL - RL - LR + RR. \end{aligned} \tag{2}$$

In Eq. (2),[25] the first letter represents the polarization state of the PSG system, and the second one corresponds to the polarization state of the PSA system. For example, in the HV image, the polarization states of the PSG and PSA systems are horizontal and vertical, respectively.

Once the Mueller matrix is calculated, we can estimate the values of the diattenuation (D),[27–29] polarizance (P),[27–29] retardance (R),[27,28] depolarization (Δ),[29] and the angle of polarization (θ)[30,31] via Eq. (3). Diattenuation is a property that describes the magnitude of the variation of the transmitted irradiance as a function of the incident polarization state.[29] Polarizance is the ability of a medium to polarize light and is usually measured through the degree of polarization of light when passing through a medium. Diattenuation and polarizance can be considered as the opposite effect. In a homogeneous medium, the polarizance and diattenuation are equal.[28] Depolarization is defined as the property of a medium to convert a polarized beam into a depolarized one.[29] The retardance map reveals the phase change induced by the sample within the EM components of the light.[27,28] We apply the polar decomposition reported by Chipman and Lu[27] to calculate the diattenuation, polarizance, retardance, and depolarization. Finally, the angle of polarization is the orientation of the transmission axis of a linear polarizer to the optical reference of the system. The polarization angle θ is only relevant if the sample has linear polarizing behavior.[31] Moreover,

$$D = \frac{\sqrt{m_{01}^2 + m_{02}^2 + m_{03}^2}}{m_{00}}, \quad P = \frac{\sqrt{m_{10}^2 + m_{20}^2 + m_{30}^2}}{m_{00}},$$

$$\Delta = 1 - \frac{\sqrt{\left(\sum_{i=0}^{3} m_{ii}^2\right) - m_{00}^2}}{\sqrt{3}m_{00}}, \quad \theta = \frac{1}{2}\tan^{-1}\left(\frac{\sqrt{m_{20}^2 + m_{30}^2}}{m_{10}}\right),$$

$$R = \cos^{-1}\left(\mathrm{Tr}\left(\frac{M}{2}\right) - 1\right). \tag{3}$$

We have implemented a numerical simulator of the polarimeter as a tool for instructors and students to review concepts before experimenting in the laboratory.[32] These numerical simulations aim to recover the same output Mueller matrix as the one used in the input sample after applying the technique. Thirty-six intensity-based images of 10 × 10 pixels are computationally generated in Python (version 3.8.5) and the Py-pol library for each input sample.[33,34] This library allows the generation of the pointwise Mueller matrix for the input sample and each polarizing element in the PSG and PSA systems. Assuming that the PSG system is composed of an LP and a QWP, and the PSA system is also composed of a QWP and the LP [Fig. 1(a)], the resulting matrix of the proposed polarimeter for an arbitrary input sample is equal to

$$M = M_{LP_{PSA}} M_{QWP_{PSA}} M_{sample} M_{QWP_{PSG}} M_{LP_{PSG}}. \tag{4}$$

Since biological and other intricate samples can present different polarization states across their field of view, we model the sample to consist of two linear polarization states oriented to +45° in the top left of the sample, −68° in the bottom left of the sample, and a quarter-wave plate with its fast axis at 0° in the right half. The Mueller matrix for each area of the input sample is

$$M_{LP_{+45^\circ}} = \begin{bmatrix} 1 & 0 & 1 & 0 \\ 0 & 0 & 0 & 0 \\ 1 & 0 & 1 & 0 \\ 0 & 0 & 0 & 0 \end{bmatrix}$$

$$M_{LP_{-68^\circ}} = \begin{bmatrix} 1 & -0.72 & -0.69 & 0 \\ -0.72 & 0.52 & 0.5 & 0 \\ -0.69 & 0.5 & 0.48 & 0 \\ 0 & 0 & 0 & 0 \end{bmatrix}$$

$$M_{QWP_{0^\circ}} = \begin{bmatrix} 1 & 0 & 0 & 0 \\ 0 & 1 & 0 & 0 \\ 0 & 0 & 0 & 1 \\ 0 & 0 & -1 & 0 \end{bmatrix}. \tag{5}$$

Figure 2 shows the estimated Mueller matrix when using the described input sample. The values of the estimated Mueller matrix in the top left of the image correspond to the ones obtained when the ideal LP is at +45°, marked by the red rectangle in Figs. 2(a) and 2(b). The values of the estimated Mueller matrix in the bottom left of the image correspond to the ones obtained when the ideal LP is at −68°, marked by the blue rectangle in Figs. 2(a) and 2(c). The values of the Mueller matrix in the right half of the image correspond to the ones obtained when the ideal QWP is oriented at 0°, marked by the green rectangle in Figs. 2(a) and 2(d). The numerical results shown in Fig. 2 validate the implemented algorithm to recover the Mueller matrix for a non-homogeneous sample whose polarimetric properties vary across its transverse field of view. This numerical implementation aims to enhance students' polarization understanding, enabling the transfer of their mathematical

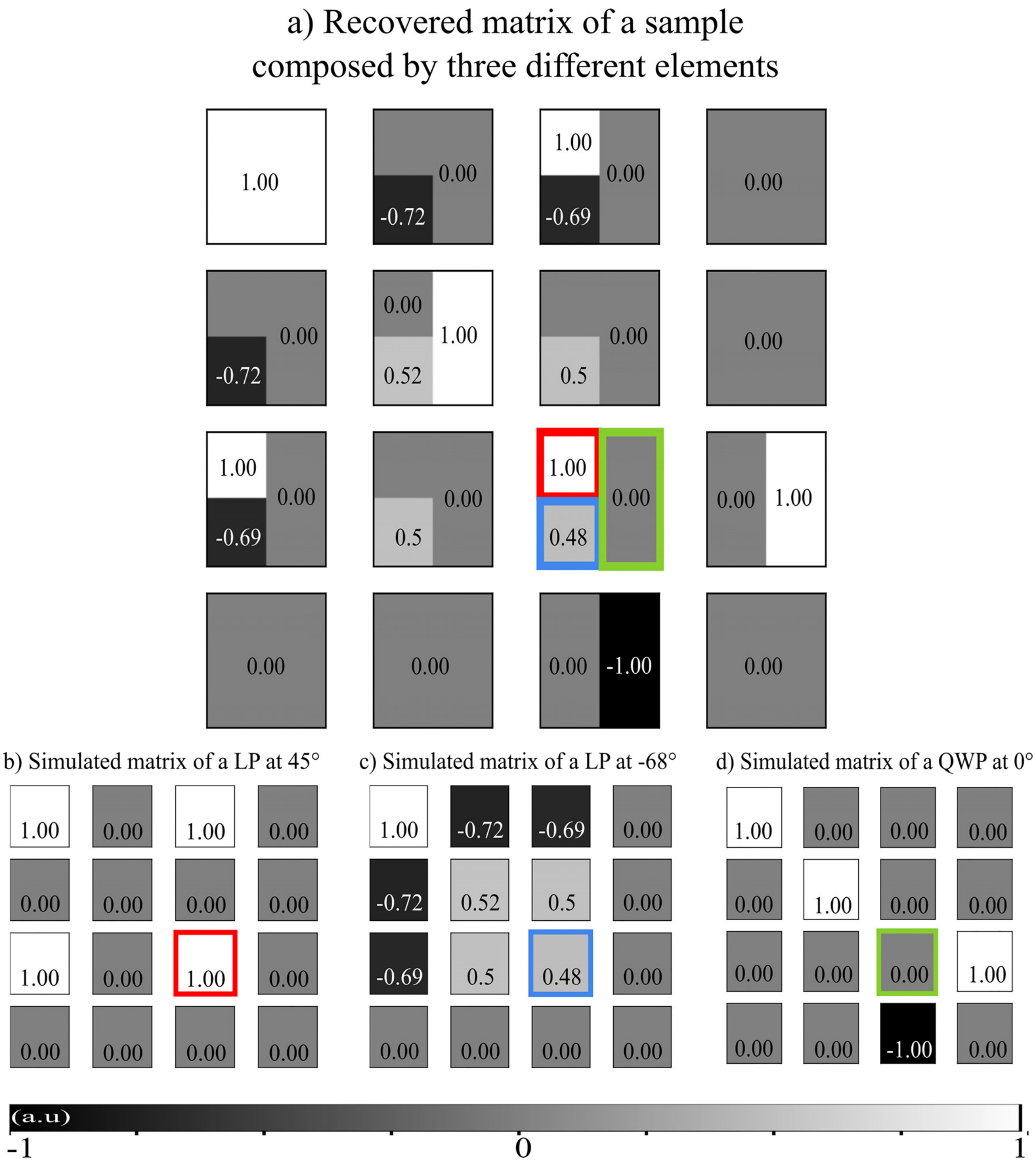
a) Recovered matrix of a sample composed by three different elements

b) Simulated matrix of a LP at 45°

1.00	0.00	1.00	0.00
0.00	0.00	0.00	0.00
1.00	0.00	1.00	0.00
0.00	0.00	0.00	0.00

c) Simulated matrix of a LP at -68°

1.00	-0.72	-0.69	0.00
-0.72	0.52	0.5	0.00
-0.69	0.5	0.48	0.00
0.00	0.00	0.00	0.00

d) Simulated matrix of a QWP at 0°

1.00	0.00	0.00	0.00
0.00	1.00	0.00	0.00
0.00	0.00	0.00	1.00
0.00	0.00	-1.00	0.00

Fig. 2. Estimated Mueller matrix of a sample composed of an ideal LP at +45° (top left of the image), −68° (bottom left of the image), and a QWP at 0° (right half of the image) using Eqs. (1) and (2).

knowledge (e.g., equations) into real applications. Therefore, students should validate the method numerically by mimicking a sample composed of linear polarizers whose transmission axes are oriented at different angles before the laboratory session.

The laboratory procedure described in this section is aimed to be followed by a student from scratch under the instructor's supervision. Depending on their level of expertise in optical instrumentation, the overall time to implement the proposed system could take between 2 h (experienced student) and 10 h (inexperienced student with basic knowledge in geometrical optics and light polarization). For an inexperienced student with basic knowledge in optics, three sessions for implementation are recommended. In the first session, the student could implement the microscope system, which will take at least 2 h. The student will build a brightfield microscope by determining the conjugated planes in an afocal system comprising an infinity-corrected microscope objective and a tube lens. The digital camera will be located at the back focal plane of the tube lens. In the second session, which will take at least 5 h, the student will implement and calibrate the polar imetric system, inserting the polarizing elements of PSG and PSA systems. The recording of the 36 brightfield microscopic images will also occur during the second session. During a final 3-h session, the student will measure the Muller matrix using the calibrated system.

III. EXPERIMENTAL RESULTS

This section is devoted to the experimental details of our brightfield microscopy approach (see Fig. 1). The sample in the experimental brightfield microscope is illuminated by light from a collimated diode-pumped solid-state (DPSS) laser with 532 nm wavelength and 4.5 mW power (Thorlabs CPS532). The microscope includes an infinity-corrected MO with a lateral magnification of 40× and a numerical aperture NA of 0.75, and a TL of 200-mm focal length. A Basler acA5472-17μm CMOS sensor (5472×3648 pixels, 2.4-μm^2 pixel size) is placed at the microscope's image plane, allowing the acquisition of focused intensity-based images. For this DPSS laser, the spot of its collimated beam is large enough to fill the sample area uniformly. The laser beam's diameter is around 3.5 mm, while the field of view (FoV) of the system is $(5472\ \text{px} \cdot 2.4\ \mu\text{m}/40\times) = 0.329\ \text{mm}$ and $(3648\ \text{px} \cdot 2.4\ \mu\text{m}/40\times) = 0.218\ \text{mm}$ in each direction. Therefore, there is no need to expand the illuminating beam spot. If using an illumination source with a small spot, an afocal system comprised of two positive lenses of different focal lengths could be used to attain the necessary illumination spot size.

The PSG and PSA systems are inserted in the microscope to provide polarization-sensitive measurements. Since the DPSS laser is elliptically polarized, there are two possibilities, as described in Sec. II A. In this case, a depolarizer (Thorlabs DPU-25-A) was used to change the polarization state from elliptical to random polarization. Thus, the polarizing elements of the PSG and PSA systems are two LP (Thorlabs LPVISE100-A) and two achromatic QWP (Thorlabs AQWP10M-580). Because these polarizing elements must rotate to record the 36 intensity-based images, the elements are mounted onto motorized rotational stages, two K10CR1/M for the LP, and two ELL14K for the QWP, both products are from Thorlabs. Appendix C provides the list of the optical elements used in this experimental setup and their costs. The use of motorized rotational mounts instead of manual rotational mounts may improve the accuracy of the measurements by avoiding precision errors while setting angular positions of the elements. We compare the performance of both rotational mounts in Sec. IV.

Before evaluating the performance of our method, users should experimentally verify if any microscope element changes the polarization state of the light beam. For this verification, apply the described technique when no sample is in the setup in order to characterize the effect of MO and TL on the polarization state of light. Figure 3 represents the experimental Mueller matrix for an anisotropic sample with a transverse section equal to $328 \times 219\,\mu\text{m}^2$ at the sample plane. Since the sample is isotropic, each Mueller element's value should be constant (within the experimental error) across the imaged area. Based on this expectation, we have averaged the values around the central part of the images in Fig. 3. This area (red rectangle in the element m_{00} in Fig. 3) encloses $256 \times 256\ \text{px}^2$, which is equivalent to $15 \times 15\,\mu\text{m}^2$ at the sample plane. The mean and standard deviations for each $256 \times 256\ \text{px}^2$ central Mueller element are calculated and reported in Fig. 3. Students may increase the size of the red rectangle at will to perform their statistical analysis. Nonetheless, the computation of the polarization properties may be tedious if one selects a larger area of the whole image.

When comparing these values to the theoretical ones of a non-polarizing element, which corresponds to the 4×4 identity matrix, the agreement between the experimental and theoretical results is evident but not perfect: An average error of 10.8% for the measured Mueller elements in Fig. 3 has been obtained. Using the central region of the Mueller matrix, marked by the red rectangle in Fig. 3, we have estimated the values of the diattenuation (D), polarizance (P), and depolarization (Δ) using Eq. (3). The experimental diattenuation, polarizance, depolarization, and retardance are 0.18 ± 0.16 a.u., 0.30 ± 0.12 a.u., -0.05 ± 0.20 a.u., and 0.18 ± 0.019 rad,

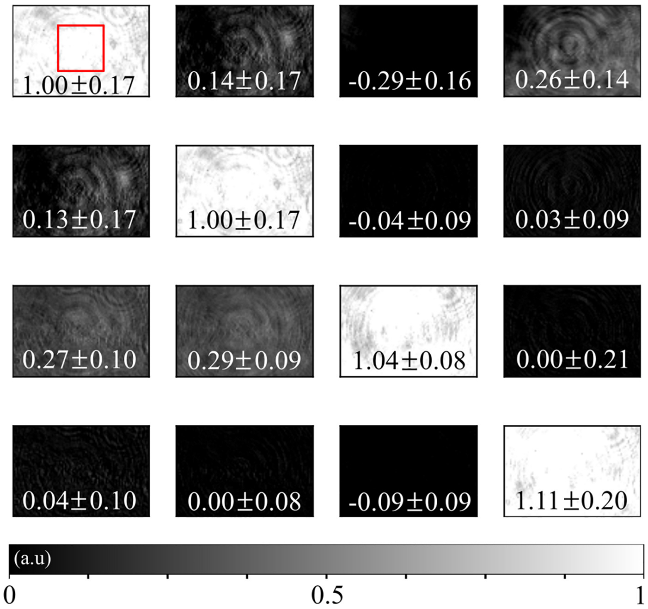

Fig. 3. Experimental Mueller matrix when no sample is present in the setup. For each element of the Mueller matrix, the mean and standard deviation across the region of the imaged field of view enclosed by the red rectangle are reported. The microscope is a nonpolarizing system.

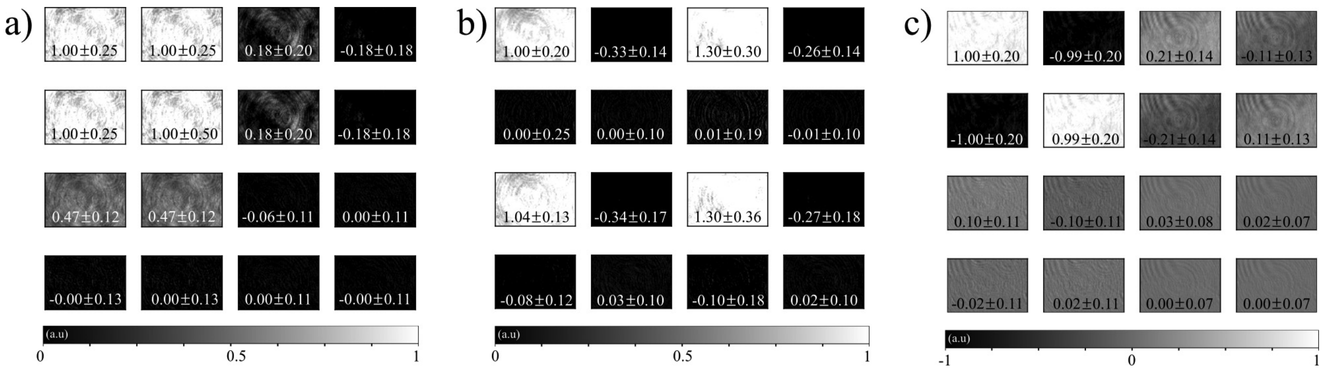

Fig. 4. Experimental Mueller matrix of a linear polarizer oriented at (a) 0°, (b) +45°, and (c) 90°. For each element of the Mueller matrix, the mean and standard deviation across the imaged field of view are shown.

respectively. The experimental uncertainty of these parameters has been estimated through uncertainty propagation and partial derivatives (see Appendix A for the equations used for these estimations). Since no lenses manufactured with anisotropic media are included in the microscope, the expected theoretical values of these three parameters are zero. While the depolarization parameter matches the theoretical expectation, the values of the diattenuation and polarizance are slightly higher than the theoretical. This disagreement may be related to the distortions in the recorded images (shown in Fig. 3) and some inaccurate orientations of the polarizing elements. Nonetheless, despite this difference, we can conclude that the microscope does not significantly affect the polarization state of the incident light.

A. Linear polarizer measurement

In the first experimental validation of our method, we use a LP (Thorlabs LPVISE 100-A) oriented at three angles: 0°, +45°, and 90°. The calculated Mueller matrices of the LP oriented at these three angles are shown in Fig. 4. The agreement between the experimental and theoretical Mueller matrices is high. Table I presents the LP's theoretical and experimental polarimetric parameters for the three orientation angles: diattenuation, polarizance, depolarization, and angle of polarization. Again, the degree of correlation between theoretical and experimental results for the LP at +45° and +90° is high. Nonetheless, there is some discrepancy for the LP at 0°. In this experiment, the retardance is not reported since this quantity will reach an undetermined value for a pure polarizer sample, as can be expected according to Eq. (3). Section IV examines potential error sources in our experimental data. The software implementation to calculate the pointwise Muller matrices from the 36 intensity-based recorded images and the corresponding polarimetric parameters can be found in Ref. 32, written both in MATLAB (tested in version 2019b) and in Python (tested in version 3.8.5).

B. Biological samples measurement

Finally, we present and discuss the experimental results on two biological samples from Carolina Biology using our apparatus. These microscopic samples are a mammal tendon slide (item No. 312788) and a mammal muscle-tendon junction slide (item no. 312806). According to the literature, tendon samples have shown polarimetric properties. The left-side panels in Fig. 5 show the brightfield images without PSG and PSA systems. Because both slides are heavily stained using haematoxylin (H&E), we cannot discriminate any sample information in these images. The regions with dark intensity values correspond to the samples' areas. However, the Mueller matrix of these biological samples provides more insight in that we can analyze each sample's polarimetric properties in highly stained areas, i.e., the regions where we could not directly see any sample information.

Figure 5 shows the polarizance, depolarization, diattenuation, and retardance maps of the sample's region enclosed by the cyan rectangle in the brightfield image. These maps were obtained using our open-access Python code in Ref. 32, which follows the method described in Sec. II. The polarimetric maps in Fig. 5 show that both samples display similar polarizing behavior. First, they do not exhibit significant depolarization. Second, they induce some degree of polarizance, diattenuation, and retardance in the incident light. This behavior agrees with that reported in Ref. 12 and validates the experimental polarization-sensitive microscope and method for characterizing the polarimetric properties of biological samples. A potential application related to this work may be identifying, classifying, and screening microscopic samples using polarization. In particular, one could integrate this approach with learning-based methods for image

Table I. Polarimetric parameters of a linear polarizer oriented at 0°, +45°, and 90°.

	LP roughly at 0°		LP roughly at +45°		LP roughly at 90°	
	Theo.	Exp.	Theo.	Exp.	Theo.	Exp.
Diattenuation (a.u.)	1	1.03 ± 0.53	1	1.31 ± 0.39	1	1.01 ± 0.37
Polarizance (a.u.)	1	1.10 ± 0.34	1	1.09 ± 0.24	1	1.05 ± 0.36
Depolarization (a.u.)	0.42	−0.17 ± 0.20	0.42	0.24 ± 0.25	0.42	0.42 ± 0.21
Angle θ (°)	0	12.65 ± 0.06	45	45.08 ± 0.37	90	89.94 ± 0.05

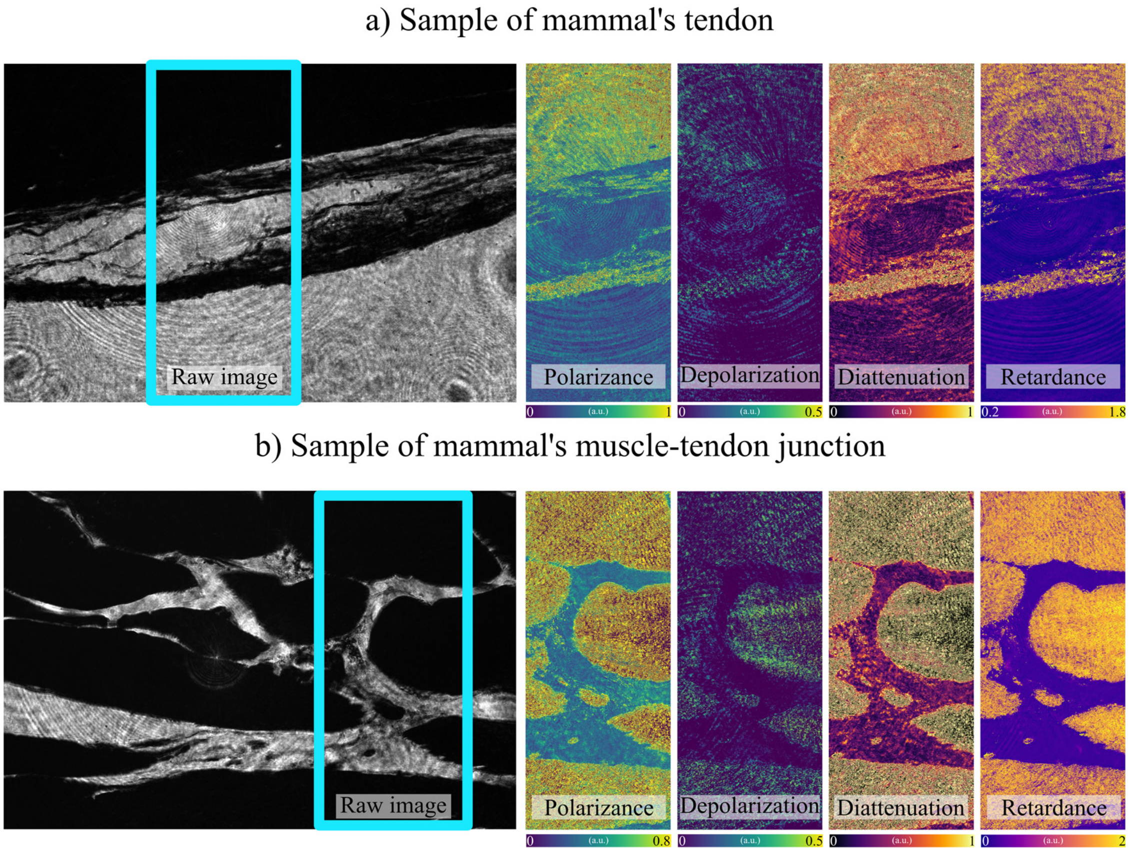

Fig. 5. Polarimetric properties of two biological samples: (a) mammal tendon and (b) mammal muscle-tendon junction.

classification, which is currently a hot topic in optics and other fields.

IV. DISCUSSION

We have presented a method for calculating the Mueller matrix of a sample based on 36 images. Although the presented experimental results have a high correlation with the theoretical ones, there are still some discrepancies. This section will provide an error analysis of the proposed technique and its instrumentation as well as discuss some recommendations for reducing these discrepancies to achieve more reliable results.

A. The illumination source

In these experiments, we employed a collimated DPSS laser module with 532 nm wavelength and 4.5 mW power (Thorlabs CPS532) as the illumination source due to its availability in the laboratory. The main inconvenience of using a coherent light source is that the recorded images are distorted by the diffraction patterns generated by any small

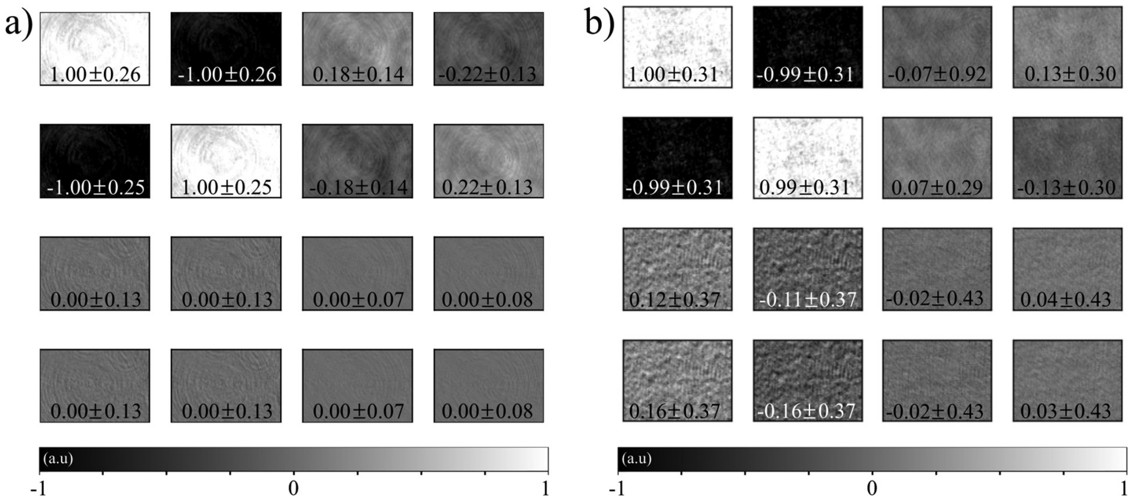

Fig. 6. Experimental Mueller matrix of a linear polarizer oriented at 90° using (a) motorized and (b) manual rotating mounts. For each element of the Mueller matrix, the mean and standard deviation across the imaged field of view are shown.

Table II. Polarimetric parameters of a linear polarizer oriented at 0° without and with the inverse-matrix correction.

		Experimental results without the correction		Experimental results after the correction	
	Theoretical prediction	Mean ± std	Error	Mean ± std	Error
Diattenuation (a.u.)	1	1.03 ± 0.35	3%	1.01 ± 0.31	1%
Polarizance (a.u.)	1	1.10 ± 0.34	10%	1.00 ± 0.24	0%
Depolarization (a.u.)	0.42	-0.17 ± 0.20	41%	0.42 ± 0.17	0%
Angle, θ (°)	0	12.65	…	4.6	…

amount of dust present in the optical elements and the speckle noise.[35] This noise source produces arbitrary changes in the recorded intensity values, disturbing the measurements. Low-coherent light sources, such as a LED,[13,36] are unaffected by high-coherence noise. Therefore, this light source could provide more homogeneous intensity images than those recorded by high-coherent sources, yielding a more accurate estimation of the Mueller matrix with the presented methodology. A collimated wavefront should illuminate the sample with our microscopic imaging system. Therefore, one should be careful to select the proper LED illumination. Suppose the selected LED source does not emit a collimated wavefront (e.g., it is a conventional LED source). In that case, additional wavefront-shaping optical elements should be inserted after the LED source to create the required collimated beam.

B. The usage of motorized mounts versus manual mounts

Our method requires a particular set of polarization states for the PSG and PSA systems. A possible cause of error in the measurement of the Mueller matrix can be the exact angular position of the polarization elements in both the PSG and PSA systems. Note that any slight deviation in the position of the PSG and PSA elements affects the intensity in the recorded image and, consequently, the calculated Mueller matrix. In our apparatus, we attached the polarization elements on motorized mounts to change the angular position of the elements.

Figure 6 shows the comparison of two Mueller matrixes from a LP at 90° using motorized mounts [Fig. 6(a)] and manual rotating mounts [Fig. 6(b)].

Although the calculated Mueller matrix using manual rotating mounts still captures the trend of the theoretical expectation, the elements present higher experimental errors (e.g., the standard deviation is higher than the one provided by the data using motorized mounts). Comparing the results shown in Fig. 6, motorized mounts have reduced both human and systematic errors due to the uncertainty in the angular position of the polarizing elements, leading to polarimetric measurements with reduced uncertainty. Therefore, motorized mounts are recommended if the quantitative Mueller matrix is used to screen and diagnose biological samples with high accuracy. Another advantage of using motorized mounts instead of manual ones is reducing the acquisition time. While an average student may take 30–45 min to record the 36 images using manual mounts, the acquisition time may be reduced to 5–7 min if the acquisition process is correctly automatized using the motorized mounts. Note that an automatic acquisition stage requires minimum student effort and intervention.

C. The inverse-matrix correction

Finally, the experimental results can be improved by using the inverse-matrix correction method.[7] This approach aims to compensate for any experimental error introduced by the system without sample, M_{system}, by calculating its inverse matrix and multiplying this result to the measured Mueller matrix, $M_{measured}$. Thus, mathematically, a corrected measured Mueller matrix is generated via $M_{correct} = M_{system}^{-1} M_{measured}$. This method is suitable when the Mueller matrix with no sample present in the setup diverges from the identity matrix as in our case (see Fig. 3). Note that if the system is perfectly nonpolarizing, its Mueller and inverse matrices would equal the identity matrix. Nonetheless, the implemented system deviates from a perfectly nonpolarizing device due to experimental errors. Therefore, we can correct these errors by compensating with the inverse Mueller matrix of the system. Table II compares the polarimetric parameters of a linear polarizer at 0° without and with inverse matrix correction. As stated before, the retardance of the linear polarizer sample is not reported nor used for the inverse-matrix correction since its insertion will generate a significant difference from the theoretical expectation.

Note that the corrected values present a smaller error with respect to the theoretical expectations, validating the goodness of the inversion-matrix approach. Table II shows the mean and the standard deviation of each polarization property and the error with respect to the theoretical value of each property. The error has been calculated with the equations presented in Appendix A.

V. CONCLUSION

In summary, we have presented a lab experience to estimate the Mueller matrix in bright-field microscopy based on the intensity-based method. The proposed method requires 36 intensity-based images in which the polarization states of the PGS and PSA systems have been changed. Before the laboratory session, students are encouraged to validate the method numerically by mimicking a sample composed of linear polarizers whose transmission axes are oriented at different angles. We have also presented a guide to build and align a polarization-sensitive microscope from a conventional brightfield microscope. The polarimetric parameters of standard linear polarizers are retrieved accurately following these guidelines. The hallmark characteristics of the proposed method are its simplicity and efficiency. The method has been implemented in PYTHON and MATLAB and is available in Ref. 32. Another advantage of the proposed method is that it allows the retrieval of the Mueller matrix across the transverse section of a sample, being suitable for analyzing biological and other intricate samples. The presented laboratory experiment will allow students to develop a deeper understanding of polarization and Mueller matrix analysis in imaging, increasing the learning opportunities of students in introductory optical laboratory courses.

ACKNOWLEDGMENTS

S. Obando-Vasquez thanks Camilo Cano-Barrera for his support and willingness to accompany the theoretical appropriation process throughout the work. C. Trujillo acknowledges the support by Vicerrectoria de Ciencia, Tecnologia e Innovacion from Universidad EAFIT. A. Doblas acknowledges the support from the National Science Foundation (NSF, No. 2042563), the University of Memphis, and the Herff College of Engineering.

AUTHOR DECLARATIONS

Conflict of Interest

The authors declare no conflicts of interest.

APPENDIX A: ESTIMATION OF UNCERTAINTY FOR POLARIMETRIC PARAMETERS

In this section, we provide the equation to estimate the uncertainty of the diattenuation (D), polarizance (P), depolarization (Δ), and angle of polarization (θ). The experimental uncertainty of these parameters depends on the uncertainty of the elements of the Mueller matrix. We have quantified the experimental uncertainty of the polarimetric parameters using partial derivatives of the measurement with respect to each of the Mueller matrix elements as follows:

$$\sigma_D = \sqrt{\left(\frac{\partial D}{\partial m_{01}}\right)^2 \sigma_{m_{01}}^2 + \left(\frac{\partial D}{\partial m_{02}}\right)^2 \sigma_{m_{02}}^2 + \left(\frac{\partial D}{\partial m_{03}}\right)^2 \sigma_{m_{03}}^2 + \left(\frac{\partial D}{\partial m_{00}}\right)^2 \sigma_{m_{00}}^2},$$

$$\sigma_P = \sqrt{\left(\frac{\partial P}{\partial m_{01}}\right)^2 \sigma_{m_{01}}^2 + \left(\frac{\partial P}{\partial m_{02}}\right)^2 \sigma_{m_{02}}^2 + \left(\frac{\partial P}{\partial m_{03}}\right)^2 \sigma_{m_{03}}^2 + \left(\frac{\partial P}{\partial m_{00}}\right)^2 \sigma_{m_{00}}^2},$$

$$\sigma_\Delta = \sqrt{\left(\frac{\partial \Delta}{\partial m_{11}}\right)^2 \sigma_{m_{11}}^2 + \left(\frac{\partial \Delta}{\partial m_{22}}\right)^2 \sigma_{m_{22}}^2 + \left(\frac{\partial \Delta}{\partial m_{33}}\right)^2 \sigma_{m_{33}}^2 + \left(\frac{\partial \Delta}{\partial m_{00}}\right)^2 \sigma_{m_{00}}^2},$$

$$\sigma_R = \sqrt{\left(\frac{\partial R}{\partial mr_{00}}\right)^2 \sigma_{mr_{00}}^2 + \left(\frac{\partial R}{\partial mr_{11}}\right)^2 \sigma_{mr_{11}}^2 + \left(\frac{\partial R}{\partial m_{22}}\right)^2 \sigma_{mr_{22}}^2 + \left(\frac{\partial R}{\partial mr_{33}}\right)^2 \sigma_{mr_{33}}^2},$$

$$\sigma_\theta = \sqrt{\left(\frac{\partial \theta}{\partial m_{10}}\right)^2 \sigma_{m_{10}}^2 + \left(\frac{\partial \theta}{\partial m_{20}}\right)^2 \sigma_{m_{20}}^2 + \left(\frac{\partial \theta}{\partial m_{30}}\right)^2 \sigma_{m_{30}}^2},$$

where $\sigma_{m_{ij}}$ is the experimental uncertainty of the element ij of the Mueller matrix and $\sigma_{mr_{ij}}$ is the experimental uncertainty of the element *ij* of the Retardance matrix (for more details about the retardance matrix and how to calculate it with the polar decomposition, see Ref. 27). After estimating the corresponding derivation, the final equations of the experimental uncertainties are

$$\begin{aligned}\sigma_D =& \left[\left(\frac{m_{01}}{m_{00}\sqrt{m_{01}^2+m_{02}^2+m_{03}^2}}\right)^2 \sigma_{m_{01}}^2 + \left(\frac{m_{02}}{m_{00}\sqrt{m_{01}^2+m_{02}^2+m_{03}^2}}\right)^2 \sigma_{m_{02}}^2 + \left(\frac{m_{03}}{m_{00}\sqrt{m_{01}^2+m_{02}^2+m_{03}^2}}\right)^2 \sigma_{m_{03}}^2\right.\\ &\left.+\left(\frac{\sqrt{m_{01}^2+m_{02}^2+m_{03}^2}}{m_{00}^2}\right)^2 \sigma_{m_{00}}^2\right]^{1/2},\end{aligned}$$

$$\begin{aligned}\sigma_P =& \left[\left(\frac{m_{10}}{m_{00}\sqrt{m_{01}^2+m_{02}^2+m_{03}^2}}\right)^2 \sigma_{m_{10}}^2 + \left(\frac{m_{20}}{m_{00}\sqrt{m_{01}^2+m_{02}^2+m_{03}^2}}\right)^2 \sigma_{m_{20}}^2 + \left(\frac{m_{30}}{m_{00}\sqrt{m_{01}^2+m_{02}^2+m_{03}^2}}\right)^2 \sigma_{m_{30}}^2\right.\\ &\left.+\left(\frac{\sqrt{m_{01}^2+m_{02}^2+m_{03}^2}}{m_{00}^2}\right)^2 \sigma_{m_{00}}^2\right]^{1/2},\end{aligned}$$

$$\begin{aligned}\sigma_\Delta =& \left[\left(\frac{m_{11}}{\sqrt{3}m_{00}\sqrt{m_{01}^2+m_{02}^2+m_{03}^2}}\right)^2 \sigma_{m_{11}}^2 + \left(\frac{m_{22}}{\sqrt{3}m_{00}\sqrt{m_{01}^2+m_{02}^2+m_{03}^2}}\right)^2 \sigma_{m_{22}}^2 + \left(\frac{m_{33}}{\sqrt{3}m_{00}\sqrt{m_{01}^2+m_{02}^2+m_{03}^2}}\right)^2 \sigma_{m_{33}}^2\right.\\ &\left.+\left(\frac{\sqrt{m_{01}^2+m_{02}^2+m_{03}^2}}{\sqrt{3}m_{00}^2}\right)^2 \sigma_{m_{00}}^2\right]^{1/2},\end{aligned}$$

$$\sigma_R = \Bigg[\left(-\frac{1}{2\sqrt{1-\left(\frac{1}{2}(mr_{00}+mr_{11}+mr_{22}+mr_{33})-1\right)^2}}\right)^2 \sigma^2_{mr_{00}}$$

$$+\left(-\frac{1}{2\sqrt{1-\left(\frac{1}{2}(mr_{00}+mr_{11}+mr_{22}+mr_{33})-1\right)^2}}\right)^2 \sigma^2_{mr_{11}}$$

$$+\left(-\frac{1}{2\sqrt{1-\left(\frac{1}{2}(mr_{00}+mr_{11}+mr_{22}+mr_{33})-1\right)^2}}\right)^2 \sigma^2_{mr_{22}}$$

$$+\left(-\frac{1}{2\sqrt{1-\left(\frac{1}{2}(mr_{00}+mr_{11}+mr_{22}+mr_{33})-1\right)^2}}\right)^2 \sigma^2_{mr_{33}}\Bigg]^{1/2},$$

$$\sigma_\theta = \Bigg[\left(\frac{\sqrt{m_{20}^2+m_{30}^2}}{2m_{10}^2\left(1+\frac{m_{20}^2+m_{30}^2}{m_{10}^2}\right)}\right)^2 \sigma^2_{m_{10}} + \left(\frac{m_{20}}{2m_{10}^2\sqrt{m_{20}^2+m_{30}^2}\left(1+\frac{m_{20}^2+m_{30}^2}{m_{10}^2}\right)}\right)^2 \sigma^2_{m_{20}}$$

$$+\left(\frac{m_{30}}{2m_{10}^2\sqrt{m_{20}^2+m_{30}^2}\left(1+\frac{m_{20}^2+m_{30}^2}{m_{10}^2}\right)}\right)^2 \sigma^2_{m_{30}}\Bigg].$$

APPENDIX B: ORIENTATION ANGLES OF THE PSG AND PSA SYSTEMS

We provide the angles of the polarization elements of both the PSG and PSA systems with respect to their zero reference. Positive orientation angles are rotated clockwise. As mentioned in the manuscript, the polarization elements of the PSG system depend on the polarization state of the illumination source, distinguishing two main cases: (1) a randomly polarized source and (2) a linearly polarized source. The orientation angles of the polarization elements for both cases are given in Tables III and IV.

Table III. Orientation angles (in degrees) of the polarizing elements using a randomly polarized source.

	Orientation angles					Orientation angles			
	LP-PSG	QWP-PSG	QWP-PSA	LP-PSA		LP-PSG	QWP-PSG	QWP-PSA	LP-PSA
ML	–45	–45	0	45	PL	45	45	0	45
MR	–45	–45	0	–45	PR	45	45	0	–45
MM	–45	–45	45	–45	PM	45	45	45	–45
MP	–45	–45	–45	45	PP	45	45	–45	45
MH	–45	–45	90	0	PH	45	45	90	0
MV	–45	–45	90	90	PV	45	45	90	90
RL	–45	90	0	45	LL	45	90	0	45
RR	–45	90	0	–45	LR	45	90	0	–45
RM	–45	90	45	–45	LM	45	90	45	–45
RP	–45	90	–45	45	LP	45	90	–45	45
RH	–45	90	90	0	LH	45	90	90	0
RV	–45	90	90	90	LV	45	90	90	90
HL	0	0	0	45	VL	90	90	0	45
HR	0	0	0	–45	VR	90	90	0	–45
HM	0	0	45	–45	VM	90	90	45	–45
HP	0	0	–45	45	VP	90	90	–45	45
HH	0	0	90	0	VH	90	90	90	0
HV	0	0	90	90	VV	90	90	90	90

Table IV. Orientation angles (in °) of the polarizing elements using a linearly polarized source.

	Orientation angles					Orientation angles			
	HWP-PSG	QWP-PSG	QWP-PSA	LP-PSA		HWP-PSG	QWP-PSG	QWP-PSA	LP-PSA
ML	–22.5	–45	0	45	PL	–22.5	45	0	45
MR	–22.5	–45	0	–45	PR	–22.5	45	0	–45
MM	–22.5	–45	45	–45	PM	–22.5	45	45	–45
MP	–22.5	–45	–45	45	PP	–22.5	45	–45	45
MH	–22.5	–45	90	0	PH	–22.5	45	90	0
MV	–22.5	–45	90	90	PV	–22.5	45	90	90
RL	–22.5	90	0	45	LL	–22.5	90	0	45
RR	–22.5	90	0	–45	LR	–22.5	90	0	–45
RM	–22.5	90	45	–45	LM	–22.5	90	45	–45
RP	–22.5	90	–45	45	LP	–22.5	90	–45	45
RH	–22.5	90	90	0	LH	–22.5	90	90	0
RV	–22.5	90	90	90	LV	–22.5	90	90	90
HL	0	0	0	45	VL	45	90	0	45
HR	0	0	0	–45	VR	45	90	0	–45
HM	0	0	45	–45	VM	45	90	45	–45
HP	0	0	–45	45	VP	45	90	–45	45
HH	0	0	90	0	VH	45	90	90	0
HV	0	0	90	90	VV	45	90	90	90

Table V. List of the optical elements and their prices.

Optical element	Reference	Manufacturer	Quantity	Unit price (USD)	Price (USD)
Laser	CPS532	Thorlabs	1	$176	$176
Depolarizer	DPU-25-A	Thorlabs	1	$736	$736
LP	LPVISE100-A	Thorlabs	2	$101	$202
Motorized rotational stages	K10CR1/M	Thorlabs	2	$1430	$2859
	ELL14K	Thorlabs	2	$561	$1121
QWP	AQWP10M-580	Thorlabs	2	$989	$1978
MO	N40X-PF	Thorlabs	1	$1373	$1373
TL	AC254-200-A-ML	Thorlabs	1	$109	$109
Camera	acA5472-17um	Basler	1	$679	$679
General components	SM1A25	Thorlabs	1	$21	$21
	SM1A39	Thorlabs	1	$21	$21
	KAD11F	Thorlabs	1	$71	$71
	CSA1001	Thorlabs	5	$321	$1,608
	CFB1500	Thorlabs	1	$684	$684
Total					$11 638

Table VI. List of the low-cost optical elements and their prices.

Optical element	Reference	Manufacter	Quantity	Unit price (USD)	Price (USD)
Laser	CPS532	Thorlabs	1	$176	$176
Depolarizer	DPU-25-A	Thorlabs	1	$736	$736
LP	LPVISE100-A	Thorlabs	2	$101	$202
Motorized rotational stages	K10CR1/M	Thorlabs	2	$1430	$2859
	ELL14K	Thorlabs	2	$561	$1121
QWP	AQWP10M-580	Thorlabs	2	$989	$1978
MO	RMS40X	Thorlabs	1	$718	$718
TL	AC254-200-A-ML	Thorlabs	1	$109	$109
Camera	acA5472-17um	Basler	1	$679	$679
General components	XT66SD-500	Thorlabs	1	$89	$89
	RCA1	Thorlabs	5	$54	$272
	KAD11F	Thorlabs	1	$71	$71
	SM1A39	Thorlabs	5	$31	$21
	SM1A3	Thorlabs	1	$19	$19
Total					$9050

APPENDIX C: ELEMENTS LIST

Table V reports the list of elements and their prices used in the polarization-sensitive microscope. This list should be seen as a reference list. Also, in Table VI, we provide a low-cost alternative elements list for a horizontal optical setup. Alternative optical elements and components may be interchanged without affecting the experimental results. However, cheaper optical elements and components, such as manual rotary stages and low-cost polarizing elements, may lead to a polarization-sensitive microscope with reduced performance. For example, the performance of low-cost polarizing elements may differ from their theoretical expectation, introducing some experimental inaccuracies. Additional inaccuracies may be introduced by replacing the motorized rotational stages by manual rotational stages. These experimental inaccuracies may be overlooked if the experiment aims for educational training.

Table V references the elements used in our experiment. Nevertheless, the experiment results do not depend on specific elements. Consider that the less expensive the optical element is, the less ideal its behavior. In other words, it is possible to experiment with cheaper QWPs and LPs, but the instructor cannot expect perfect behavior. If the instructor is interested in teaching purposes only, using less expensive elements, such as manual rotary stages, is also recommended.

[a] ORCID: 0000-0003-0448-376X.

[b] Electronic mail: catrujilla@eafit.edu.co, ORCID: 0000-0002-1007-5028.

[1] E. Hecht, *Optics*, 4th ed. (Addison Wesley, New York, 2002).

[2] M. Bass, *Handbook of Optics Vol 2: Devices, Measurements, and Properties*, 2nd ed. (McGraw-Hill, New York, 1994).

[3] P. S. Theocaris and E. E. Gdoutos, *Matrix Theory of Photoelasticity*, 1st ed. (Springer-Verlag, Berlin, Heidelberg, 1979).

[4] A. Lanin and I. Fedik, *Thermal Stress Resistance of Materials* (Springer, Berlin, Heidelberg, 2008).

[5] M. W. Davidson and M. Abramowitz, "Optical microscopy," Encycl. Imaging Sci. Technol. **2**, 1–41 (2002).

[6] J. M. Rodríguez, "Polarización de la luz: Conceptos básicos y aplicaciones en astrofísica," Rev. Bras. Ensino Fís. **40**(4), 5–6 (2018).

[7] M. J. Lopera and C. Trujillo, "Linear diattenuation imaging of biological samples with digital lensless holographic microscopy," Appl. Opt. **61**(5), B77–B82 (2022).

[8] T. Colomb, F. Durr, E. Cuche, P. Marquet, H. G. Limberger, R. P. Salath, and C. Depeursinge, "Polarization microscopy by use of digital holography: Application to optical-fiber birefringence measurements," Appl. Opt. **44**(21), 4461–4469 (2005).

[9] B. Bai, H. Wang, T. Liu, Y. Rivenson, J. FitzGerald, and A. Ozcan, "Pathological crystal imaging with single-shot computational polarized light microscopy," J. Biophotonics **13**(1), e201960036 (2020).

[10] D. F. McAllister, "Stereo and 3-D display technologies," Encycl. Imaging Sci. Technol. **2**, 1–293 (2002).

[11] M. Bass, *Handbook of Optics: Volume I-Geometrical and Physical Optics, Polarized Light, Components and Instruments*, 3rd ed. (McGraw-Hill Professional, New York, 2010).

[12] J. Wang, L. Dong, H. Chen, and S. Huang, "Birefringence measurement of biological tissue based on polarization-sensitive digital holographic microscopy," Appl. Phys. B **124**(12), 1–9 (2018).

[13] Y. Wang, H. He, J. Chang, N. Zeng, S. Liu, M. Li, and H. Ma, "Differentiating characteristic microstructural features of cancerous tissues using Mueller matrix microscope," Micron **79**, 8–15 (2015).

[14] J. F. de Boer, T. E. Milner, M. J. C. van Gemert, and J. S. Nelson, "Two-dimensional birefringence imaging in biological tissue using phase and polarization sensitive optical coherence tomography," Opt. Lett. **22**(12), 934–936 (1997).

[15] F. Palacios, O. Font, G. Palacios, J. Ricardo, M. Escobedo, L. Ferreira Gomes, I. Vasconcelos, M. Muramatsu, D. Soga, A. Prado, and V. Jos, "Phase and polarization contrast methods by use digital holographic microscopy: Applications by different types of biological samples," in *Holography-Basic Principles and Contemporary Applications* (Intech Open, Rijeka, 2013).

[16] C. W. Pirnstill and G. L. Cot, "Malaria diagnosis using a mobile phone polarized microscope," Sci. Rep. **5**(1), 1–13 (2015).

[17] S. C. Gladden, "An experiment on Malus' law for the elementary laboratory," Am. J. Phys. **18**(6), 395–395 (1950).

[18] P. J. Ouseph, K. Driver, and J. Conklin, "Polarization of light by reflection and the Brewster angle," Am. J. Phys. **69**(11), 1166–1168 (2001).

[19] B. Schaefer, E. Collett, R. Smyth, D. Barrett, and B. Fraher, "Measuring the Stokes polarization parameters," Am. J. Phys. **75**(2), 163–168 (2007).

[20] J. Park, H. Yu, J.-H. Park, and Y. Park, "LCD panel characterization by measuring full Jones matrix of individual pixels using polarization-sensitive digital holographic microscopy," Opt. Express **22**(20), 24304–24311 (2014).

[21] M. Bass, *Handbook of Optics, Volume I: Geometrical and Physical Optics, Polarized Light, Components and Instruments* (McGraw-Hill, New York, 1996).

[22] S. Aknoun, P. Bon, J. Savatier, B. Wattellier, and S. Monneret, "Quantitative retardance imaging of biological samples using quadri-wave lateral shearing interferometry," Opt. Express **23**, 16383–16406 (2015).

[23] J. F. de Boer, C. K. Hitzenberger, and Y. Yasuno, "Polarization sensitive optical coherence tomography: A review," Biomed. Opt. Express **8**(3), 1838–1873 (2017).

[24] X. Li and G. Yao, "Mueller matrix decomposition of diffuse reflectance imaging in skeletal muscle," Appl. Opt. **48**(14), 2625–2631 (2009).

[25] K. Dev and A. Asundi, "Mueller-Stokes polarimetric characterization of transmissive liquid crystal spatial light modulator," Opt. Lasers Eng. **50**(4), 599–607 (2012).

[26] L. V. Wang and H.-I. Wu, *Biomedical Optics: Principles and Imaging* (Wiley, New York, 2009).

[27] R. A. Chipman and S.-Y. Lu, "Interpretation of Mueller matrices based on polar decomposition," J. Opt. Soc. Am. A **13**(5), 1106–1113 (1996).

[28] C. A. Cano Barrera, "Diseno e implementacion de un microscopio de luz polarizada para la medicion cuantitativa de propiedades polarimetricas en muestras biologicas," Ph.D. thesis (Universidad EAFIT, 2018). http://hdl.handle.net/10784/12466.

[29] R. A. Chipman, "Polarimetry," in *Handbook of Optics* (McGraw-Hill, New York, 1994), Chap. 22.

[30] E. Garcia-Caurel, R. Ossikovski, M. Foldyna, A. Pierangelo, B. Drevillon, and A. De Martino, "Advanced mueller ellipsometry instrumentation and data analysis," in *Ellipsometry at the Nanoscale*, edited by M. Losurdo and K. Hingerl (Springer, Berlin, Heidelberg, 2013), pp. 31–143.

[31] J. J. G. Perez, *Determination of Polarization Parameters in Matricial Representation, Theoretical Contribution and Development of an Automatic Measurement Device* (University of Zaragoza, Zaragoza, 1983).

[32] S.Obando-Vasquez, A. Doblas, and C. Trujillo, "Muller-matrix-microscopy" <https://oirl.github.io/Muller-Matrix-Microscopy/>.

[33] L. M. Sanchez-Brea and J. Del Hoyo, "py-pol, python module for polarization optics" <https://pypi.org/project/py-pol/>.

[34] J. del Hoyo, L. M. Sanchez-Brea, and A. Soria-Garcia, "Open source library for polarimetric calculations py-pol," Comput. Opt. **11875**, 12–20 (2021).

[35] J. W. Goodman, *Speckle Phenomena in Optics: Theory and Applications*, 2nd ed. (SPIE, 2020).

[36] O. Arteaga, M. Baldrís, J. Antó, A. Canillas, E. Pascual, and E. Bertran, "Mueller matrix microscope with a dual continuous rotating compensator setup and digital demodulation," Appl. Opt. **53**(10), 2236–2245 (2014).